



Mechanism and experimental evaluation on surface morphology of GCr15SiMn with ultrasonic vibration grinding

Daohui Xiang¹ · Binghao Li¹ · Chongyang Zhao¹ · Xiaofei Lei¹ · Peicheng Peng¹ · Zhaojie Yuan¹ · Guofu Gao¹ · Feng Jiao¹ · Bo Zhao¹

Received: 25 April 2023 / Accepted: 18 May 2023 / Published online: 2 June 2023
© The Author(s), under exclusive licence to Springer-Verlag London Ltd., part of Springer Nature 2023

Abstract

GCr15SiMn is a kind of bearing steel material with good physical and mechanical properties, which is broadly used in aerospace, automotive, and other advanced manufacturing fields. However, the harsh environment of the ordinary grinding (OG) process, including high grinding forces, high grinding temperatures, fast grinding wheel wear, and severe chip sticking, has led to the GCr15SiMn material being unable to be widely adopted. This paper introduces ultrasonic vibration grinding (UVG) technology to improve its machined surface quality. First, the formation mechanism of the two grinding methods was analyzed theoretically, and surface morphology of ultrasonic vibration grinding and ordinary grinding processing was analyzed by numerical simulation, while the effects of different processing variables on surface roughness were investigated experimentally. The results show that the simulated morphology is consistent with the experimental morphology. The grinding marks of UVG are wavy, wide, and shallow, and OGs are horizontal, with narrow and deep grooves. Also it was found that ultrasonic vibration grinding could improve the quality of the surface with lower roughness than normal grinding, and the surface roughness was reduced by more than 27%. The feed rate and spindle speed had significant effects on the surface roughness, accounting for 44.37% and 33.66%, respectively.

Keywords Ultrasonic vibration grinding · Numerical simulation · Roughness

1 Introduction

In recent years, with the progress of science and technology, various hard-to-process materials are emerging, which bring great challenges to the field of machinery manufacturing. As a new-type bearing steel material, GCr15SiMn is widely used in the manufacture of high precision rolling bearings, and the addition of silicon and manganese elements has greatly improved its comprehensive mechanical properties. However, the high hardness of GCr15SiMn leads to a difficult machining process that is extremely difficult to handle, especially during grinding, and it is difficult to guarantee its surface quality after grinding. Many scholars have done investigations to improve the performance requirements of GCr15SiMn workpieces during grinding and to enhance their surface morphology after machining.

The research found that the ordinary grinding process has many shortcomings, therefore, it is necessary to explore new technologies. Ultrasonic vibration grinding technology which combines ordinary grinding with ultrasonic vibration is a new technology [1–8]. This new technology enables effective reduction of cutting forces, machining heat, and tool wear, thus inhibiting surface damage [9–13], and also improves the quality of machined surfaces [14] and extends the service life of grinding wheels [15].

Hou et al. [16] conducted internal grinding hardening tests on GCr15 material and discussed the role of machining parameters on the surface hardness that should increase the depth of cut and grinding wheel speed from the perspective of increasing HPD. Chen et al. [17] studied ultrasonic grinding and ordinary grinding experiments on silicon carbide pottery, and they discovered that ultrasonic vibrations reduced tooth-induced scratches and microcracks on the grinding surface. Experimental results by Lakhdari F et al. [18] indicated that the application of ultrasonic vibration not only significantly improved the surface machining quality but also effectively reduced depth of the machined

✉ Daohui Xiang
dhxiang@hpu.edu.cn

¹ School of Mechanical and Power Engineering, Henan Polytechnic University, Jiaozuo 454000, Henan, China

surface damage layer; compared with ordinary grinding, the depth of sub-surface damage produced in ultrasonic vibration grinding could be reduced by about 35%. Jia et al. [19] found less adhesion and material flaking of workpieces in ultrasonic vibration grinding compared to ordinary grinding. Xiang et al. [20] studied the surface characteristics and critical toughness of nanoscale ZrO₂ ceramics under ultrasonic vibratory grinding and ordinary grinding conditions. The results showed that ultrasonic vibratory grinding could obtain high-efficiency nanosurface. Yuan et al. [21] designed a flat plate vibration device and conducted ultrasonic vibration cutting and ordinary cutting tests, which found that the number of cutting serrations increased with increasing amplitude and vibration size, as well as the formation mechanism of an ultrasonic surface is more complex, and ultrasonic vibration stages promote better-cutting performance of materials. The final machined surface will produce some textures. Wang et al. [22] developed a model for surface forming of engineering ceramics using rotary ultrasonic vibration grinding. It was shown that a simulation and adjustment of ultrasonic energy control or grinding parameters were found to control the surface shape. Finally, a theoretical model for simulation and laboratory verification was performed, and it was found that the simulated surface was highly consistent with the machined surface characteristics, which verified the correctness of the theoretical derivation. Cheung et al. [23] provided a model for artificial surface turning simulation to evaluate the influence of tool oscillation on final topography.

As a conclusion, less research has been done by scholars in recent years on the surface formation mechanism of ultrasonically processed GCr15SiMn materials. In order to research the effect of ultrasonic vibration on the grinding mechanism in GCr15SiMn material, this paper presented a predictive simulation of the morphology of GCr15SiMn material after ultrasonic vibration grinding; through experiments, the influences of ultrasonic vibration grinding on roughness and each processing parameter on roughness were explored, which provided a reference for subsequent research.

2 Materials and methods

2.1 Grinding grain track analysis

In the processing, a grinding wheel's numerous abrasive grains come into direct contact with the workpiece's surface, and the grain movement directly affects the surface quality, so it is crucial to explore the mechanics of the abrasive grains. According to the idea that macroscopic grinding is based on microscopic removal mechanisms [24], an analysis of a motion trajectory can provide insight into the microscopic removal mechanism. As mentioned in the "Introduction" section, the trajectory of the abrasive grains is changed after the addition of ultrasonic vibration, and it is necessary to analyze it.

Figure 1(a) is a schematic diagram of grinding with abrasive wheels, for which the abrasive grains are in direct contact with workpiece, and the relative motion of grinding wheel and a workpiece is in reverse orientation. As can be seen in Fig. 1(b), ultrasonic vibration is applied to the tool in an axial direction. OG is ordinary grinding, and UVG is ultrasonic vibration grinding.

As the tangential direction of grinding is determined as y and the axial direction as z , the equations of the trajectory of a single grain of abrasive are defined as follows:

$$\begin{cases} x = r_s - r_s \cos(w_s t) \\ y = v_w t + r_s \sin(w_s t) \\ z = 0 \end{cases} \quad (1)$$

$$\begin{cases} x = r_s - r_s \cos(w_s t) \\ y = v_w t + r_s \sin(w_s t) \\ z = A \sin(wt + \varphi) \end{cases} \quad (2)$$

In this model, r_s represents the radius of grinding wheel, w_s shows circular frequency of ultrasonic vibration, w is initial phase of extrasonic radiation, and φ shows the initial

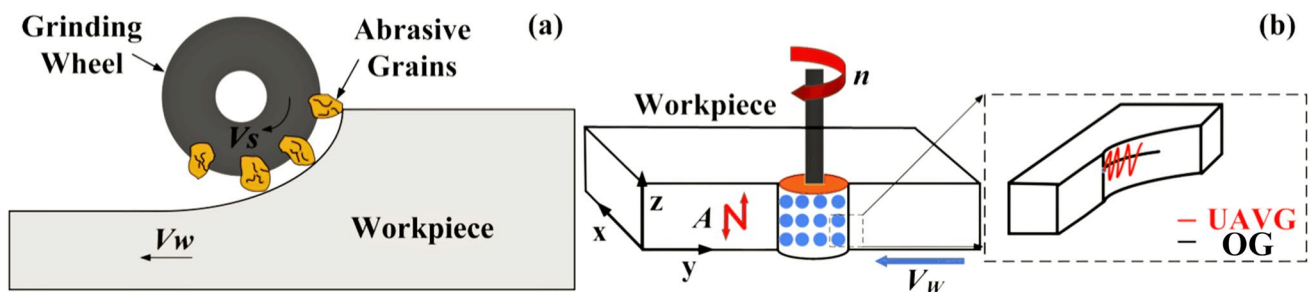


Fig. 1 Grinding diagram: (a) Abrasive grinding model (b) Ultrasonic vibration-assisted grinding model

phase of ultrasonic vibration. A is ultrasonic amplitude, t represents time, and workpiece feed rate is V_w .

Equations (1) and (2) show that there are different states of abrasive grains in the “ z ” dimension between ultrasonic vibration grinding and ordinary grinding. In ordinary grinding, the speed of abrasive grains in z -direction is 0, but in ultrasonic vibration grinding, with the addition of vibratory, there is an additional reciprocating motion of the abrasive grit in the z -direction with amplitude A , which causes the ultrasonic processing motion to be more complex. To further analyze the motion characteristics in single-grit abrasives assisted by ultrasonic vibration, the motion track curves of single-grit abrasives under two grinding conditions were plotted by numerical simulation software. As shown in Fig. 2, it is clear to see that the movement path of mill grains under ultrasonic conditions is very different from that of ordinary mill grains, which has a linear movement path, but a sinusoidal movement path under ultrasonic vibration grinding.

In ordinary grinding, the path of individual grinding grains is a horizontal line, so the ordinary grinding trajectories between grains are parallel to each other, however, ultrasonic vibration grinding transforms original grain trajectory

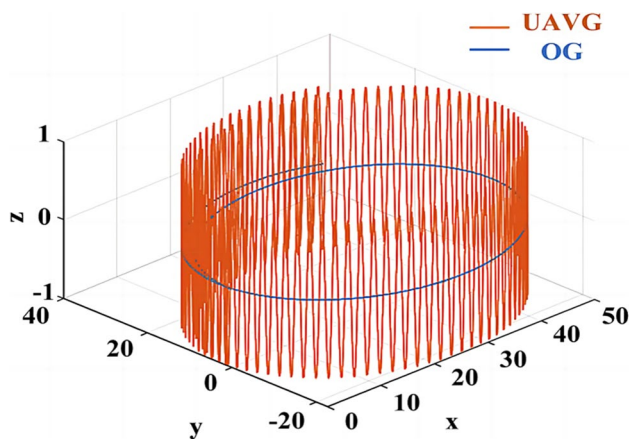
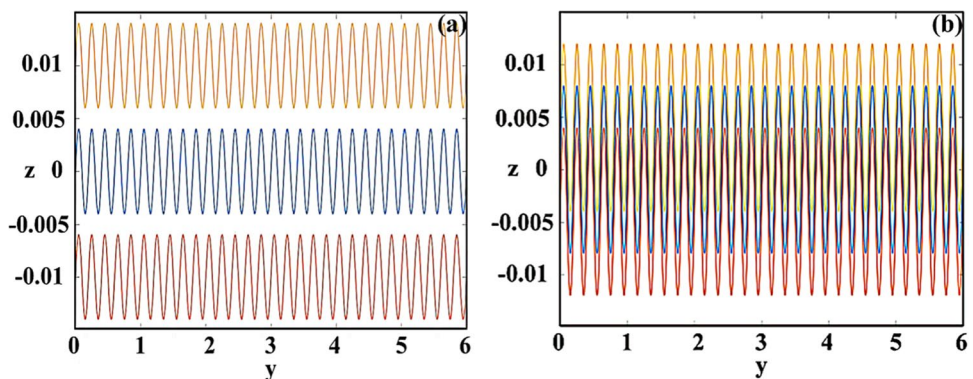


Fig. 2 Abrasive particle trajectory

Fig. 3 Adjacent abrasive grain trajectories: **a** no interference; **b** interference



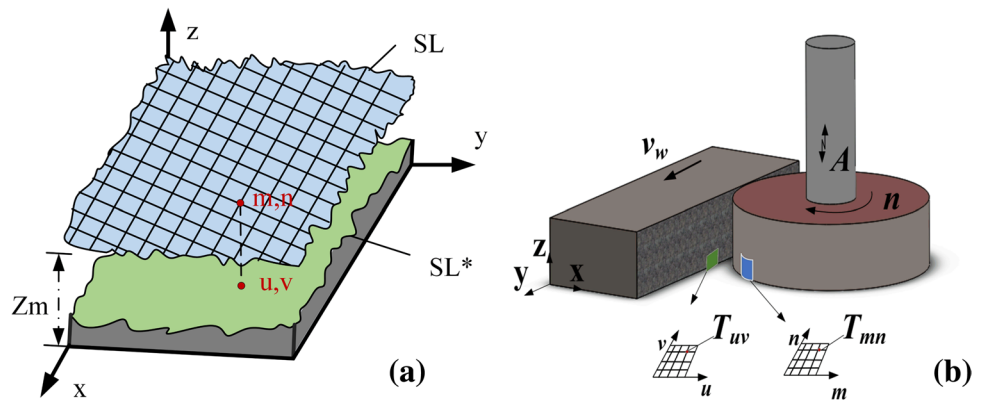
by applying ultrasonic high-frequency oscillation, which leads to a different mechanism of grinding surface formation compared with ordinary grinding, with surfaces that cross and overlap each other. Figure 3 represents particle trajectories along the axial direction between adjacent abrasive grains, and Fig. 3(a) expresses particle trajectories if the distance d between abrasive grains is greater over the ultrasonic amplitude A . At this time, there is no interference between two adjacent abrasive grains, and no overlapping and crossing of abrasive trajectories, so that the working surface will have a residual height that has not been removed. Figure 3(b) displays an orbit motion when the spacing d between the abrasives is less than ultrasonic amplitude A . At this time, it can be observed that motion paths of abrasive grit elements superpose each other, and different abrasive grains will grind and iron the same area of the workpiece several times. When the ultrasonic amplitude increases, the interference overlap between the abrasive grains will be more obvious, which is equivalent to grinding the workpiece more times, so that the right size of ultrasonic amplitude can obtain excellent performance grinding surface quality.

2.2 Numerical simulation of morphology

The surface profile after machining is very important to the performance, and naturally, the surface profile is different because of the change in the trajectory of the grinding grain. The movement paths of all particles are analyzed to obtain the traces of abrasive particles on machined surfaces of the workpiece. Firstly, Fig. 4(a) displays that the grinding wheel and part have meshed to form the mesh planes of the grinding wheel and part, represented by the topological matrices SL and SL^* , respectively. This is the grinding process as shown in Fig. 4(b). T_{uv} refers to residual height at workpiece (u, v) and T_{mn} is the height of grits protruding from grinding wheel surface at (m, n) . The minimum height Z_c of grits after moving at each grid point is calculated as the residual height after machining.

The whole grinding process is refined to the direct contact of m th particle on n th xoy surface with the workpiece, and

Fig. 4 a Grid division diagram; b surface formation diagram



the path movement of grits is known from the literature [25] as follows:

$$X_{mn(t)} = r_s + r_s \sin(w_s t - \frac{\pi}{2}) + h(m, n) - a_p \tag{3}$$

$$Y_{mn(t)} = r_s \cos(w_s t - \frac{\pi}{2}) + v_w (t + \frac{l_r}{w_s r_s}) \tag{4}$$

$$Z_{mn(t)} = A \sin(w(t + \frac{l_r}{w_s r_s}) + \frac{\pi}{2}) + n - 1 \tag{5}$$

Since grinding is the direct contact and cutting between grits and workpieces, the collection of lowest trajectory for grits can be expressed as a grinding surface. This paper analyzed and stored the trajectories of all abrasive grains on all surfaces to get a small range of grinding morphology, and

the complete grinding surface can be obtained by performing the above operations in sequence, that is,

$$H_{uv} = \min[Z_m(i, j)] + \Delta c + a_{pi} + \Delta \tag{6}$$

where Δc is abrasive grain concession value, a_{pi} is the abrasive wear value, Δw is the workpiece material recovery value, and the simulation steps are as follows:

According to Fig. 5 of the simulation process, suitable parameters were selected. With an ultrasonic amplitude of $4 \mu\text{m}$, an ultrasonic rate was 35 kHz, a speed of spindle was 4000 r/min, a grinding depth of $4 \mu\text{m}$ and feed speed was 200 mm/min. The simulated surface shapes are illustrated in Fig. 6. The surface of ordinary grinding is mainly parallel to each other, while the surface of grinding under ultrasonic conditions is relatively curved gullies as can be seen from Fig. 6(a) and (b), and the residual height of the surface of

Fig. 5 Simulation process diagram

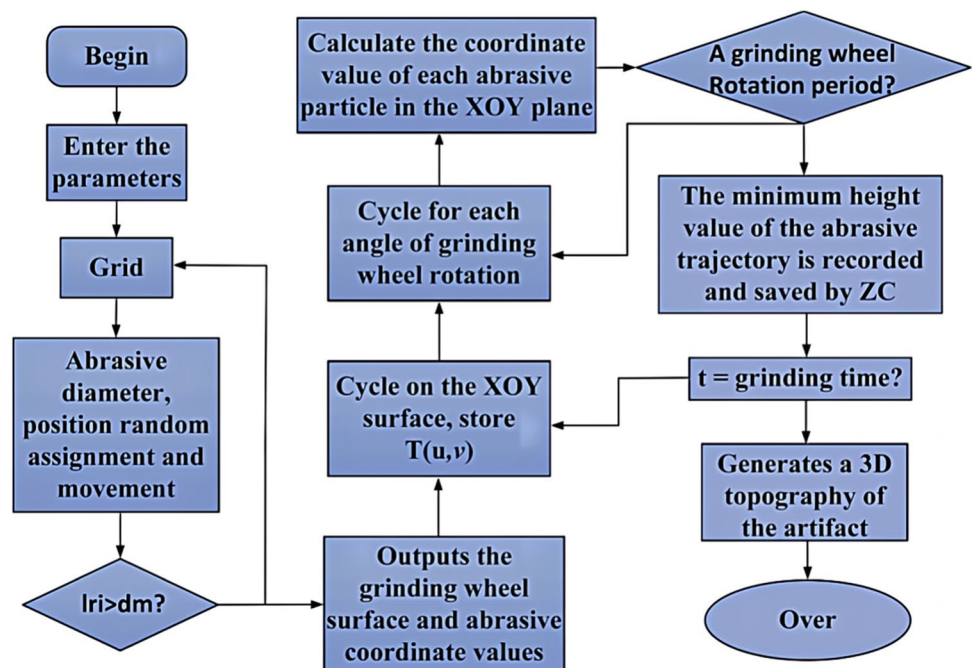
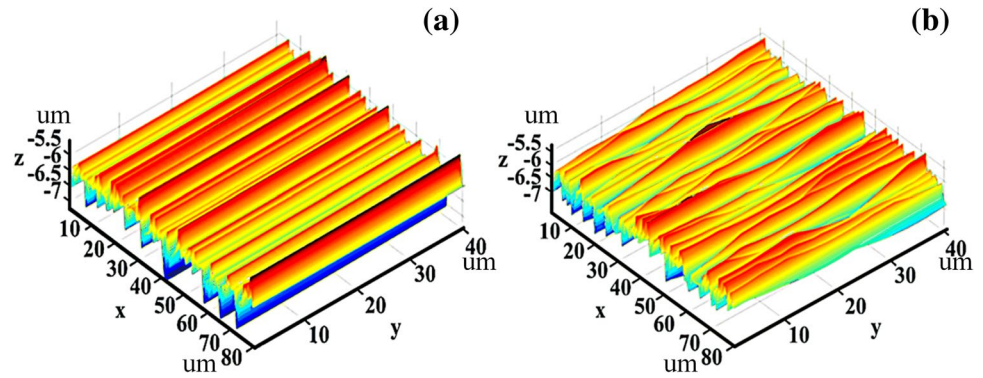


Fig. 6 Simulated topography of ground surface: **a** ordinary grinding; **b** ultrasonic vibration grinding



ordinary grinding is higher than that of ultrasonic vibration grinding under same machining parameters, and the height difference is relatively large.

3 Experimental preparation and program

The experimental workpiece is GCr15SiMn bearing steel, and its main components are listed in Table 1, and the experimental tool with a CBN grinding wheel of ceramic bond, which can reduce the loss of ultrasonic vibration energy and improve the vibration effect.

This paper built an ultrasonic vibration-assisted grinding test system as shown in Fig. 7(a). It includes a machine spindle, a wireless transmission device, an intelligent generator (SZ12, operating frequency 26–33 kHz), a piezoelectric longitudinal transducer (35 kHz), and a cylindrical-taper-cylindrical composite variable amplitude rod. The ANSYS FEM program is used to conduct modal analysis of designed three-stage composite variable rods to observe whether they have suitable resonant frequencies and longitudinal vibration modes. The simulation analysis results after adjustment and optimization in Fig. 7(b) are shown. In the cloud diagram of simulation model figure, it can be observed that the end of the variable amplitude rod produces a more obvious longitudinal vibration mode phenomenon, while the vibration displacement in between is very small. The resonant rate is within an operating frequency range of the ultrasonic generator, which can meet the experimental requirements.

Impedance analysis study of vibration systems through impedance analyzer PV70A, Fig. 7(c), demonstrates an impedance analysis of the grinding wheel tool, and as can be seen in this diagram, the resonant frequency is about 35.2 kHz, which is very close to 35.1 kHz in the above modal analysis, and the conduction circle is more round and

the vibration band is moderate. Therefore, the vibroacoustic system has a good vibration condition around the resonant frequency of 35.2 kHz, and the vibrational acoustic system meets the test requirements. As shown in Fig. 7(d), the overall UA is stable when measured with a KEYENCELK-G10 laser shift transducer. As can be seen from the local magnification, the vibration pattern curve is a smooth sine wave, which indicates the excellent stability of the designed vibration system.

As shown in Fig. 8, this test in three-axis vertical machining center (model: VMC850E) set up an independent ultrasonic experiment platform, the specific experimental protocol is displayed in Table 2.

4 Results and discussion

First of all, the surface shape of the test specimen was observed after the test, and the two-dimensional and three-dimensional morphologies under the two grinding methods were obtained, as shown in Fig. 9.

The workpiece morphology after the test is consistent with the above simulation morphology. The surface of ordinary grinding is mainly composed of parallel grooves, and the motion trajectory is relatively simple. However, the grinding surface under ultrasonic conditions is “wavy,” the grooves are relatively curved and complex, the fluctuation in depth is small, and the edge elevation is not obvious. Ultrasonic vibration grinding produces sinusoidal grinding marks on the surface; the interference between adjacent abrasive trajectories makes different abrasive particles repeatedly grind the same area for the workpiece surface, which corresponds to a secondary or multiple grinding process, reducing the bulge on both sides of the groove, which can effectively reduce the re-image of abrasive on surface of workpiece,

Table 1 GCr15SiMn bearing steel composition (mass fraction%)

C	Si	Mn	P	S	Cr	Mo	Ni	Cu	Fe
0.95–1.05	0.45–0.75	0.95–1.25	0.025	1.40–1.65	1.40–1.65	0.10	0.25	0.25	Residuals

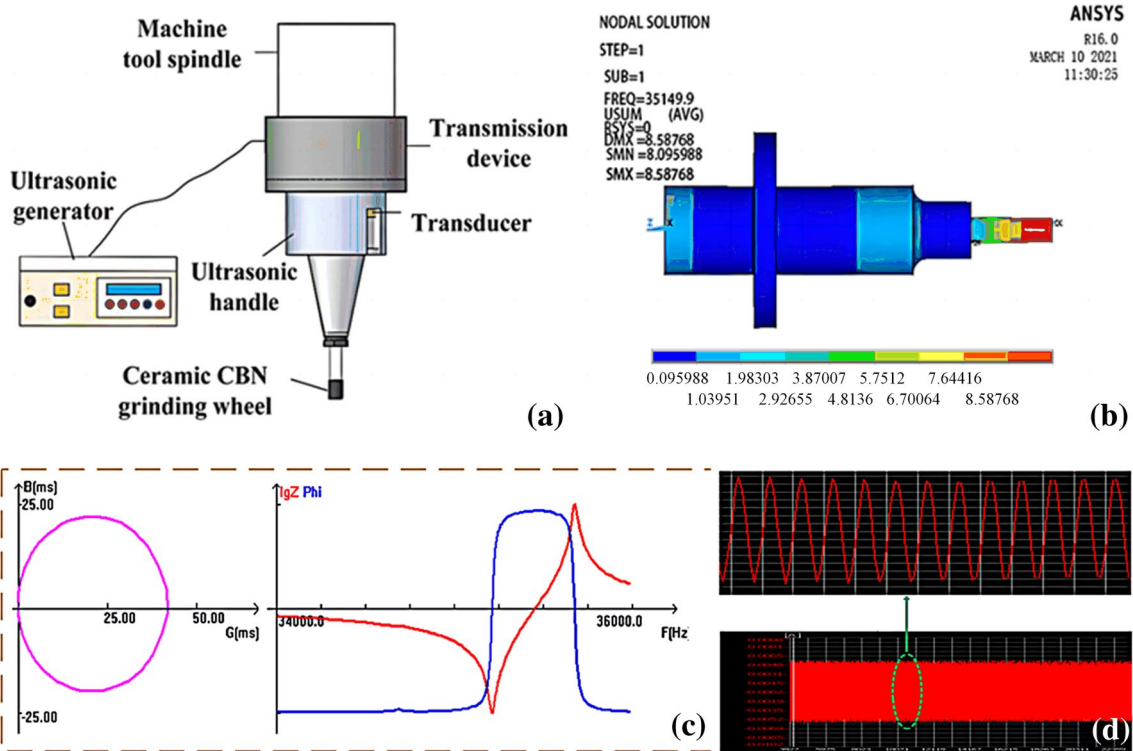


Fig. 7 a Ultrasonic vibration system, b variable amplitude rod modal analysis, c impedance analysis, and d UA test impedance analysis

improving machining accuracy and making the machining surface more flat. The increase in ultrasonic frequency and amplitude will increase the overlap of abrasive track and make additional improvements in surface quality.

To study the surface quality after the two processes, this paper observed the surface quality of the workpiece using

FEM SEM. Figure 10 provides the morphology observed with SEM. As clearly seen in Fig. 10(a), the surface grooves of ordinary grinding are narrow and deep, and the extruded material piles up on both sides of the abrasive grain trajectory. In Fig. 10(b), ultrasonic grinding surface grooves are wide and shallow. With the introduction of ultrasonic

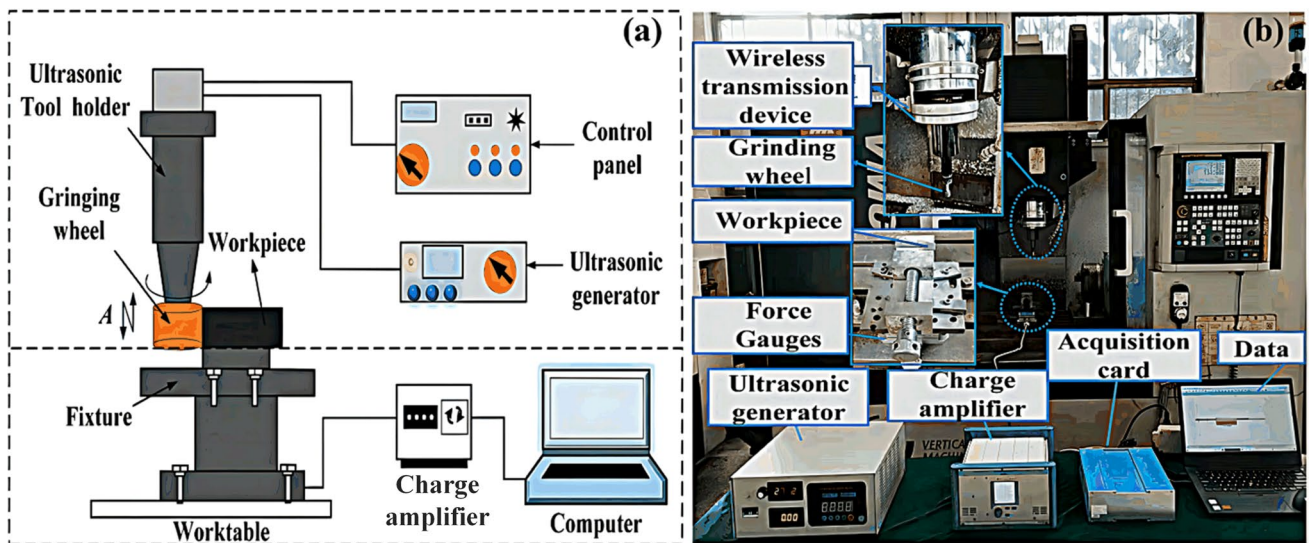


Fig. 8 Grinding test diagram: a schematic diagram and b site diagram

Table 2 Test scheme

Grinding method and processing parameters	Experimental conditions
Grinding process	General grinding, ultrasonic vibration grinding
Grinding wheel grit number	200#
Cooling type	Dry grinding
Spindle speed (r/min)	3000, 4000, 5000, 6000
Grinding depth (μm)	2, 4, 6, 8
Feeding speed (mm/min)	100, 150, 200, 250
Ultrasonic amplitude (μm)	0, 2, 4, 6

vibration in ordinary grinding, it will impact deep grooves and interfere with each other in the trajectory of the abrasive grains, thus enabling the grooves and high ridges in the grinding marks to be significantly reduced. So, the surface is smoother and flatter. According to Fig. 10(c), serious tearing is also found on the ordinary grinding surface, and in Fig. 10(d), although there is also tearing on the grinding surface under ultrasonic conditions, the area is smaller

and milder. On the one hand, ultrasonic vibration decreases the temperature of grinding contact area and reduces the possibility of workpiece material adhering to the grinding wheel surface, decreasing the chance of large area tearing on workpiece surface, on the other hand, ultrasonic vibration reduces the grinding force during the grinding process, thus reducing the deformation of workpieces, and at the same time, the cross overlap of abrasive grain trajectory will grind the same area for several times, making the grinding surface relatively flat and smooth.

Roughness is a significant evaluation argument for surface quality and serves as an important technical indicator of the functionality of engineered components. The original roughness curves obtained by two grinding methods with the same parameters are displayed in Fig. 11(a) and (b), respectively. Significant differences in surface roughness profile between ordinary grinding and ultrasonic vibration grinding can be clearly seen: For ordinary grinding, the curve fluctuates greatly, with multiple spikes and the overall appearance is relatively chaotic. For ultrasonic vibration grinding, the curve line is relatively flat, the number of spikes is less, the fluctuations of the curve are smaller, and the roughness is relatively

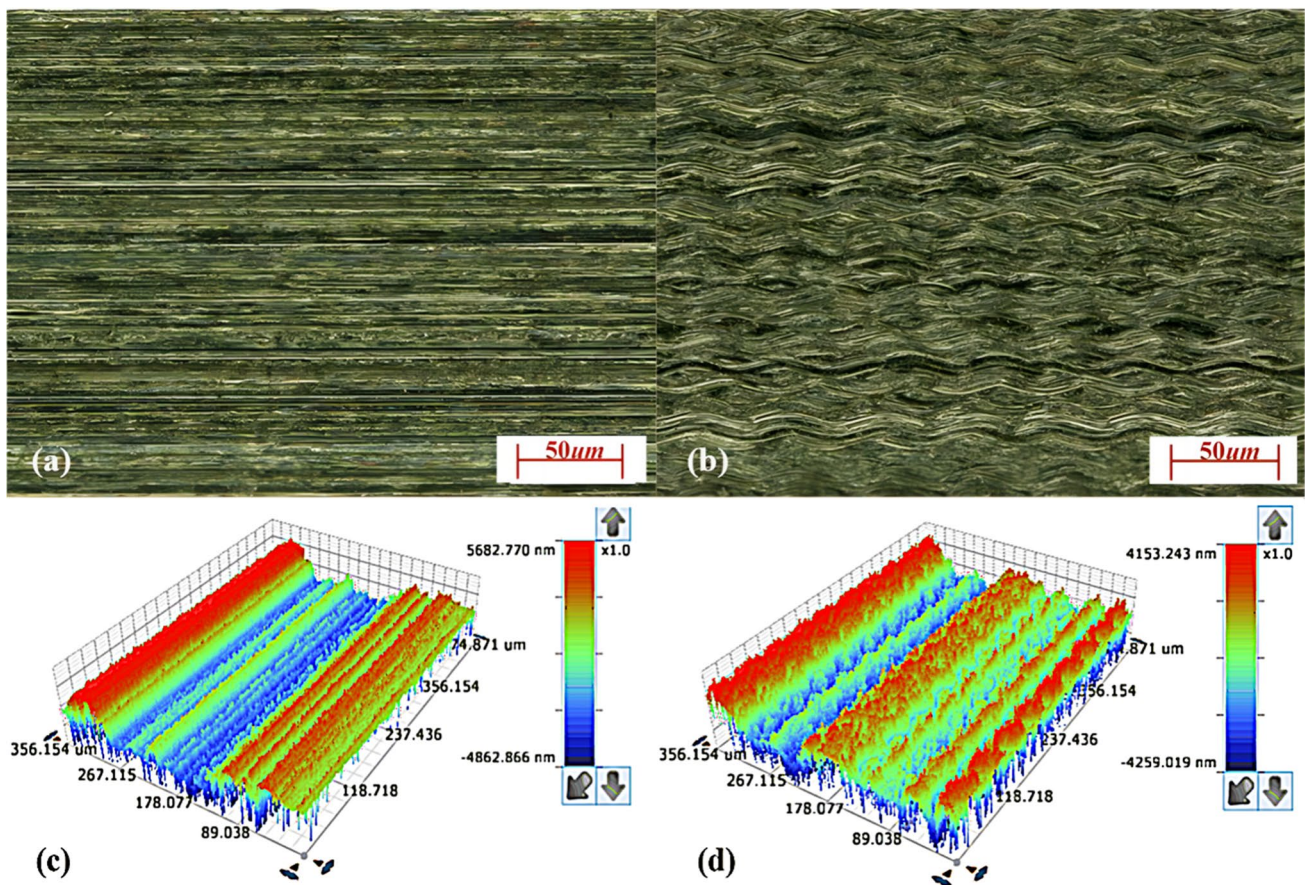


Fig. 9 surface topography: **a** ordinary grinding two-dimensional morphology; **b** ultrasonic vibration grinding two-dimensional morphology; **c** ordinary grinding three-dimensional morphology; **d** ultrasonic vibration grinding three-dimensional topography

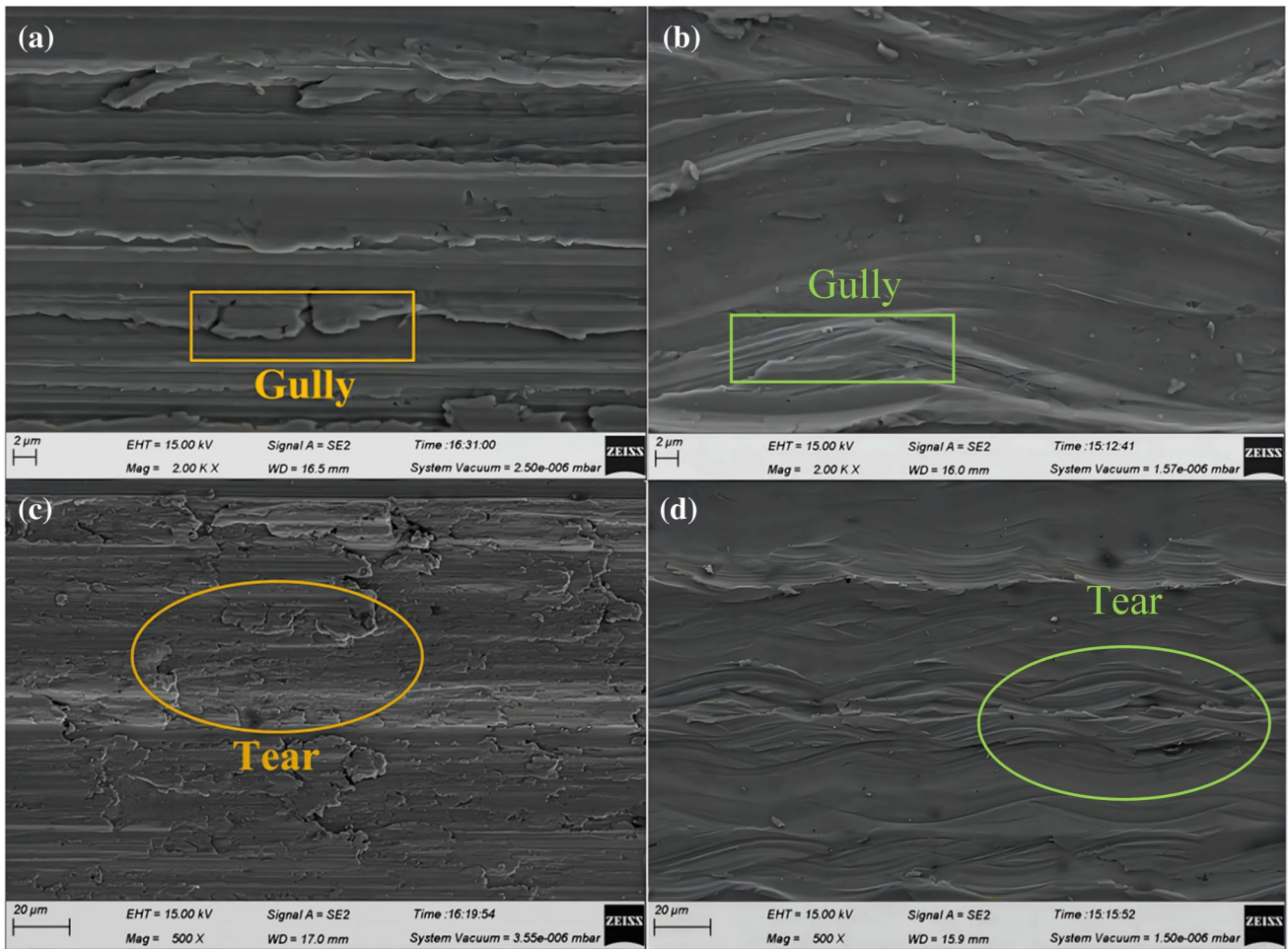


Fig. 10 Scanning electron microscopy of two processing methods: **a, c** Ordinary grinding; **b, d** ultrasonic vibration grinding

low. This is mainly attributed to the subjecting of neighboring grits with each other by ultrasonic amplitude during ultrasonic vibration grinding, the overlap and intersection of grits' trajectories, and high-frequency repetitive polishing of the grinding surface by grits in grinding area, which will again grind the bumps produced by plowing during workpiece surface grinding. Therefore, ultrasonic vibration grinding has a lower residual height of the entire machined surface than ordinary grinding surfaces.

Table 3 shows an analysis of variance for roughness, which indicates that feed speed has the most significant effect on surface roughness, followed by spindle speed, while the ultrasonic amplitude and grinding depth have little effect on surface roughness values. Figure 12 illustrates the sensitivity for different machining parameters for surface roughness, the significant ratio of feed speed reached 44.37%, the significant ratio of spindle speed was 33.66%, and the significant ratios of ultrasonic amplitude and grinding depth were 16.33% and 5.13%, respectively.

Fig. 11 Roughness profile graph: **a** ordinary grinding; **b** ultrasonic vibration grinding

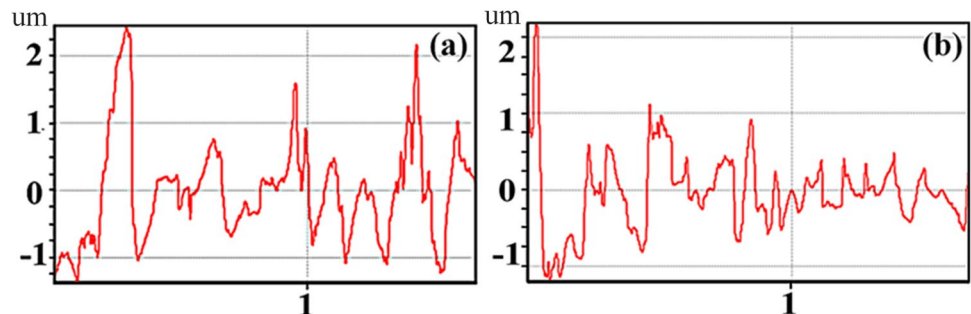


Table 3 Surface roughness orthogonal test results analysis of variance

Factor	Bias squares	Freedom	F ratio	Significance
Spindle speed	0.066	3	11.000	Significant
Grind depth	0.010	3	1.667	No significant
Feed speed	0.087	3	14.500	Significant
Amplitude	0.033	3	5.500	No significant
Error	0.01	3		

Checking the table gives: $F_{0.05}(3,3)=9.28$

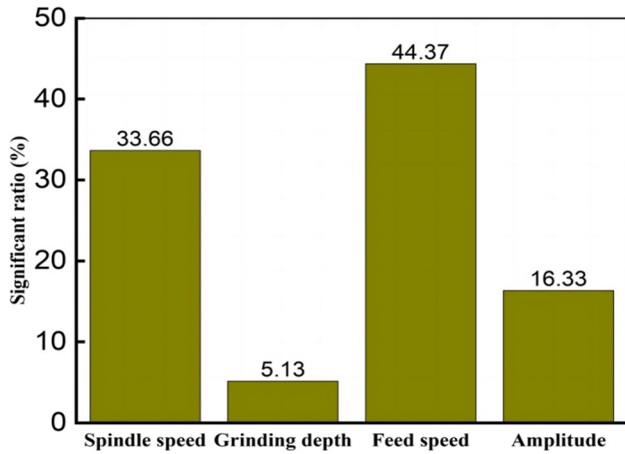
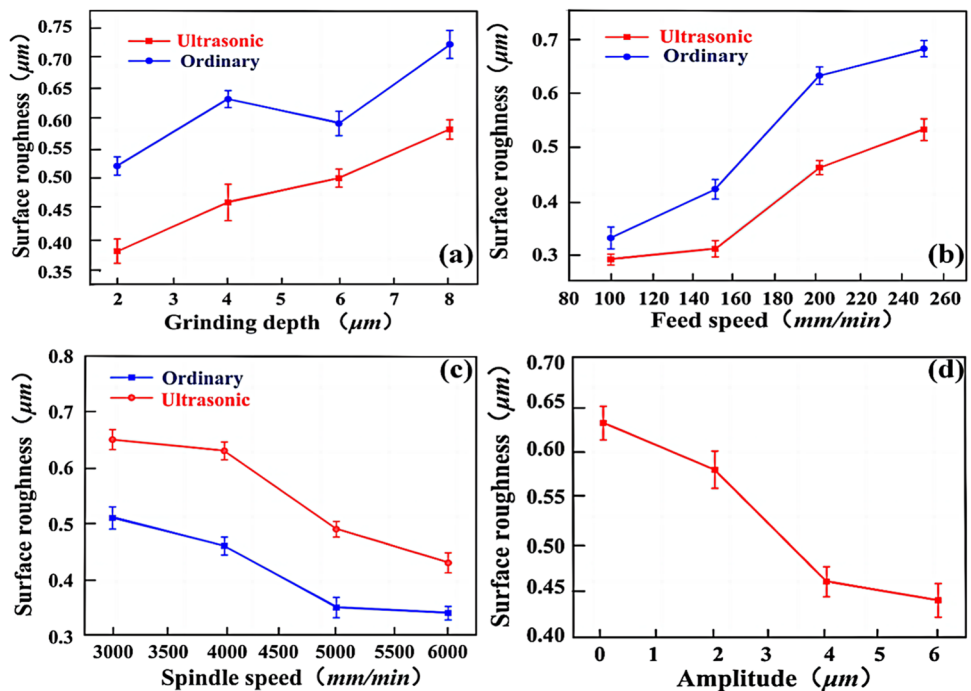


Fig. 12 Proportion of effect with different machining parameters on surface roughness

Investigation of variation pattern of roughness with processing factors using single-factor test, Fig. 13(a), indicates the influence relation of grinding depth and roughness; it can be clearly found that the roughness of both processes shows an increasing trend with the increase of grinding depth, Because, with increasing grinding depth, the radial grinding force will also rise; when it exceeds a critical wear value, the grinding state will change and impact vibration of the grits on workpiece surface will increase, the vibration will impact processed surface, and so tiny pits will appear on the surface, which will further increase the roughness. Compared with ordinary grinding, the surface roughness under ultrasonic conditions is relatively smaller, and the rising trend is relatively gentle with increasing depth. Because ultrasonic vibration grinding causes the motion trajectory to cross and superimpose since HF vibrations are applied, different abrasive grains grind and iron the surface several times; in addition, ultrasonic high-frequency vibration produces a certain softening effect to workpiece surface, which improves machinability of the workpiece and leads to more ductile removal of the material, which enhances the surface finish and further reduces the roughness.

As indicated in Fig. 13(b), which displays the variation between different feed speeds and apparent surface finish, when feed speed increases, the surface roughness under both grinding methods tends to increase; this is because an increase in feed speed will result in a larger average chip thickness of the grits, which will lead to greater interaction between the workpiece and the grits, resulting in plow lines and wrinkles on workpiece surfaces and serious burrs and bumps on both sides of the grooves created by grits. Under the same parameters, ultrasonic vibration overlaps the tracks of neighboring

Fig. 13 Effect of each machining parameter on roughness: **a** effect of grinding depth; **b** effect of feed speed; **c** effect of spindle speed; **d** effect of ultrasonic amplitude



grits on the grinding wheel surface, and the adjacent particles will polish burrs and bumps several times, meanwhile, the surface of workpiece will produce a coating phenomenon under the action of ultrasonic waves, thus reducing the roughness of surface grinding.

The curve of surface finish variation at different spindle rotation rates is depicted in Fig. 13(c); with increasing spindle speed, the surface roughness for both grinding processes follows a decreasing trend, and the surface roughness under ultrasonic conditions is smaller. Since higher rotational velocity leads to an improvement in the amount of effective abrasive grains for identical material volume removal, the mean cutting thickness of abrasive grains decreases, resulting in smaller plastic deformation in the process of tillage and plowing, meanwhile, with increasing grit numbers, multiple regrinds of the same area on a surface can be performed per unit of time, thus the surface is more finish. Oscillation of ultrasonic action can lead to overlap between abrasive tracks as well, the number of grinding in the same area is further increased, and the surface is extruded and polished, which effectively raises the smoothness of a surface. Furthermore, ultra-sonographic oscillation facilitates the discharge of grinding chips and dislodged abrasive particles, so that the possibility of grinding burns and scratches on workpiece surface is reduced, thus enabling greater surface quality.

Figure 13(d) illustrates a profile of change between different ultrasonic amplitudes and surface roughness. Visible, ultrasonic vibration grinding can significantly reduce surficial roughening compared with ordinary grinding, which has zero ultrasonic amplitude. As the amplitude grows, an overlapping phenomenon of grits strengthens, the overlap rate of grinding traces interacting with each other in the grinding area increases, and the concave valleys and convex peaks at surface become smoother; therefore, a significant reduction for the surficial roughening. When the ultrasonic amplitude beyond 4 μm continues to increase, the roughness decreases slowly, which is because the ultrasonic vibration produces a certain impact; it will bring a larger extrusion and friction, and workpiece deformation is increased, instead, further reduction of roughness is inhibited. Compared with ordinary grinding, when the ultrasonic amplitude was 6 μm , it was found that the maximum reduction of surface roughness under ultrasonic conditions was about 27%, indicating that the ultrasonic-assisted grinding with appropriate amplitude is effective in diminishing surface roughness.

5 Conclusions

This paper analyzed the machining mechanisms of the two processes by individual abrasive grain trajectories in the two grinding processes and explored the effect law of machining parameters on roughness through 3D morphological simulation results for both processes, eventually obtaining the following conclusions:

- (1) According to the results of MATLAB, the trajectory of ordinary grinding is horizontal, and the motion trajectory of ultrasonic vibration grinding is more complex, with overlapping cutting trajectories of ultrasonic vibration grinding in adjacent grinding grains, and the significance of this phenomenon is a positive correlation with ultrasonic amplitude.
- (2) The surface profile of the numerical simulation matched the experimental surface profile, which proved the reliability of the simulation, and it was found that the surface profile of ultrasonic vibration grinding was wide and shallow compared with the ordinary grinding which was narrow and deep, and the surface damage was less compared with the ordinary grinding.
- (3) In comparison with ordinary grinding, the surface mass of ultrasonic vibration grinding has fewer spikes and almost no damage to the surface, and the surface of ultrasonic vibration also benefits from the reduction of surface roughness. The feed speed and spindle rotation rate significantly influenced the surface roughness with at 44.37% and 33.66%, respectively, while the ultrasonic amplitude and grinding depth have a smaller effect on the roughness, with significant ratios of 16.33% and 5.13%, respectively. The surface roughness showed the same trend changes as grinding depth and feed rate increased, in contrast to trends of spindle speed and ultrasonic amplitude. Ultrasonic vibration grinding can bring down the surface roughness by up to over 27% for ordinary grinding.

Author contribution Daohui Xiang: project administration, formal analysis, writing—review and editing. Binghao Li: methodology, investigation, and formal analysis. Chongyang Zhao: data curation and investigation. Xiaofei Lei: data curation and investigation. Peicheng Peng: data curation and investigation. Zhaojie Yuan: data curation and investigation. Guofu Gao: writing—review and editing. Feng Jiao: writing—review and editing. Bo Zhao: writing—review and editing.

Funding This work was supported by the National Natural Science Foundation of China [grant numbers 51975188]; the Henan Provincial Science and Technology Research Project [grant number 222102220005]; the Henan Provincial Science and Technology Research Project [grant number 212102210056]; the Special Funds for Basic Scientific Research Business Expenses of Henan Universities [grant number NSFRF200102].

Data availability Data and materials are available.

Code availability Not applicable.

Declarations

Ethics approval Not applicable.

Consent to participate Not applicable.

Consent for publication All authors have read and agreed to the published version of the manuscript.

Conflict of interest The authors declare no competing interests.

References

- Wang H, Hu YB, Cong WL, Hu ZL (2019) A mechanistic model on feeding-directional cutting force in surface grinding of CFRP composites using rotary ultrasonic machining with horizontal ultrasonic vibration. *Int J Mech Sci* 155:450–460. <https://doi.org/10.1016/j.ijmecsci.2019.03.009>
- Cao Y, Yin JF, Ding WF, Xu JH (2021) Alumina abrasive wheel wear in ultrasonic vibration-assisted creep-feed grinding of Inconel 718 nickel-based superalloy. *J Mater Process Technol* 297:117241. <https://doi.org/10.1016/j.jmatprotec.2021.117241>
- Jia D, Li C, Zhang Y, Yang M, Zhang X, Li R, Ji H (2019) Experimental evaluation of surface topographies of NMQL grinding ZrO₂ ceramics combining multiangle ultrasonic vibration. *Int J Adv Manuf Technol* 100:457–473. <https://doi.org/10.1007/s00170-018-2718-y>
- Dong S, Dapino MJ (2017) Dynamic system model for ultrasonic lubrication in perpendicular configuration. *Ultrasonics* 75:98–105. <https://doi.org/10.1016/j.ultras.2016.11.010>
- Yang ZC, Zhu LD, Zhang GX, Ni CB, Lin B (2020) Review of ultrasonic vibration-assisted machining in advanced materials. *Int J Mach Tools Manuf* 156:103594. <https://doi.org/10.1016/j.ijmactools.2020.103594>
- Gao T, Zhang XP, Li CH, Zhang YB, Yang M, Jia DZ, Ji HJ, Zhao YJ, Li RZ, Yao P, Zhu LD (2020) Surface morphology evaluation of multi-angle 2D ultrasonic vibration integrated with nanofluid minimum quantity lubrication grinding. *J Manuf Process* 51:44–61. <https://doi.org/10.1016/j.jmapro.2020.01.024>
- Yang Y, Yang M, Li C, Li R, Said Z, Ali HM, Sharma S (2023) Machinability of ultrasonic vibration assisted micro-grinding in biological bone using nanolubricant. *Front Mech Eng* 18:1–10. <https://doi.org/10.1007/s11465-022-0717-z>
- Chen HF, Tang JY, Shao W, Zhao B (2018) An investigation of surface roughness in ultrasonic assisted dry grinding of 12Cr2Ni4A with large diameter grinding wheel. *Int J Precis Eng Manuf* 19(6):929–936. <https://doi.org/10.1007/s12541-018-0110-3>
- Ning FD, Cong WL (2020) Ultrasonic vibration-assisted (uv-a) manufacturing processes: state of the art and future perspectives. *J Manuf Process* 51:174–190. <https://doi.org/10.1016/j.jmapro.2020.01.028>
- Verma G C, Pandey P M, Dixit U S (2018) Modeling of static machining force in axial ultrasonic-vibration assisted milling considering acoustic softening. *Int J Mech Sci* 136. <https://doi.org/10.1016/j.ijmecsci.2017.11.048>
- Zhou WH, Tang JY, Chen HF, Shao W (2019) A comprehensive investigation of surface generation and material removal characteristics in ultrasonic vibration assisted grinding. *Int J Mech Sci* 156:14–30. <https://doi.org/10.1016/j.ijmecsci.2019.03.026>
- Wang H, Hu YB, Cong WL, Hu ZY, Wang YQ (2020) A novel investigation on horizontal and 3d elliptical ultrasonic vibrations in rotary ultrasonic surface machining of carbon fiber reinforced plastic composites. *J Manuf Process* 52:12–25. <https://doi.org/10.1016/j.jmapro.2020.01.027>
- Zhao M, Zhu J, Song S, Xue B, Zhao B (2022) Influence of machining parameters in longitudinal-torsional ultrasonic vibration milling titanium alloy for milling force. *Int J Adv Manuf Technol* 1–11. <https://doi.org/10.1007/s00170-022-10509-4>
- Peng PC, Xiang DH, Li YQ, Yuan ZJ, Lei XF, Li B, Liu GF, Zhao B, Gao GF (2022) Experimental study on laser assisted ultrasonic elliptical vibration turning (la-uevt) of 70% SiCp/Al composites. *Ceram Int* 48(22):33538–33552. <https://doi.org/10.1016/j.ceramint.2022.07.298>
- Ding K, Fu YC, Su HH, Gong XB, Wu KQ (2014) Wear of diamond grinding wheel in ultrasonic vibration-assisted grinding of silicon carbide. *Int J Adv Manuf Technol* 71(9):1929–1938. <https://doi.org/10.1007/s00170-014-5625-x>
- Hou D P, Gao S X, Liu J D, Huang S W (2020) Effect of grinding parameters on the hardness penetration depth of the steel GCr15 in internal grind hardening process. *Journal of physics. Conference series*, p 12112. <https://doi.org/10.1088/1742-6596/1637/1/012112>
- Chen YR, Su HH, Qian N, He JY, Gu JQ, Xu JH, Ding K (2021) Ultrasonic vibration-assisted grinding of silicon carbide ceramics based on actual amplitude measurement: grinding force and surface quality. *Ceram Int* 47(11):15433–15441. <https://doi.org/10.1016/j.ceramint.2021.02.109>
- Lakhdari F, Bouzid D, Belkhir N, Herold V (2019) Surface and subsurface damage in zerodur® glass ceramic during ultrasonic assisted grinding. *Int J Adv Manuf Technol* 90(5):1993–2000. <https://doi.org/10.1016/j.jmapro.2019.01.046>
- Jia DZ, Li CH, Zhang YB, Yang M, Zhang XP, Li RZ, Ji HJ (2019) Experimental evaluation of surface topographies of nmql grinding zro2 ceramics combining multiangle ultrasonic vibration. *Int J Adv Manuf Technol* 100(1):457–473. <https://doi.org/10.1007/s00170-018-2718-y>
- Xiang D H, Yue G X, Zhi X T, Gao G F, Zhao B (2011) Study on cutting force and tool wear of high volume SiC/Al MMCs with ultrasonic vibration high speed milling. *Key Eng Mater*, p 264–268. <https://doi.org/10.4028/www.scientific.net/KEM.455.264>
- Yuan ZJ, Gao GF, Wang Y, Fu ZX, Xiang DH (2022) Experimental study on a two-dimensional ultrasonic vibration platform and milling of Ti2AlNb intermetallic alloy. *Int J Adv Manuf Technol* 121(5):4187–4208. <https://doi.org/10.1007/s00170-022-09625-y>
- Wang Y, Guangheng DY, Zhao JN, Dong YH, Zhang XF, Jiang XM, Lin B (2019) Study on key factors influencing the surface generation in rotary ultrasonic grinding for hard and brittle materials. *J Manuf Process* 38:549–555. <https://doi.org/10.1016/j.jmapro.2019.01.046>
- Cheung CF, Lee WB (2000) Modelling and simulation of surface topography in ultra-precision diamond turning. *Proc Inst Mech Eng Part B-J Eng Manuf* 214(6):463–480. <https://doi.org/10.1243/0954405001517775>
- Lei XF, Xiang DH, Peng PC, Liu GF, Li B, Zhao B, Gao GF (2022) Establishment of dynamic grinding force model for ultrasonic-assisted single abrasive high-speed grinding. *J Mater Process Technol* 300:117420. <https://doi.org/10.1016/j.jmatprotec.2021.117420>
- Wang Y, Li DY, Guo LJ, Song HL, Peng SP, Wang R (2018) Prediction and experimental verification of workpiece surface topology in axial ultrasonic vibration assisted grinding based on dynamic profile sampling method. *J Mech Eng* 54(21):221–230. <https://doi.org/10.3901/JME.2018.21.221>

Publisher's note Springer Nature remains neutral with regard to jurisdictional claims in published maps and institutional affiliations.

Springer Nature or its licensor (e.g. a society or other partner) holds exclusive rights to this article under a publishing agreement with the author(s) or other rightsholder(s); author self-archiving of the accepted manuscript version of this article is solely governed by the terms of such publishing agreement and applicable law.